Available online at www.sciencedirect.com
SCIENCE DIRECT®
Journal of Solid State Chemistry 177 (2004) 3505–3513
JOURNAL OF SOLID STATE CHEMISTRY
http://elsevier.com/locate/jssc

Structures of $LiCaAlF_6$ and $LiSrAlF_6$ at 120 and 300 K by synchrotron X-ray single-crystal diffraction

Satoru Kuze,[a] Douglas du Boulay,[b] Nobuo Ishizawa,[b,*] Nobuhiro Kodama,[c] Mitsuo Yamaga,[d] and Brian Henderson[e]

[a] *Interdisciplinary School of Science and Engineering, Tokyo Institute of Technology, 4259 Nagatsuta, Midori, Yokohama 226-8502, Japan*
[b] *Ceramics Research Laboratory, Nagoya Institute of Technology, Asahigaoka, Tajimi 507-0071, Japan*
[c] *Department of Materials Science and Engineering, Faculty of Engineering and Resource Science, Akita University, Akita 010-8502, Japan*
[d] *Department of Mathematical and Design Engineering', Faculty of Engineering, Gifu University, Gifu 501-1193, Japan*
[e] *Semiconductor Physics, Cavendish Laboratory, University of Cambridge, CB3 0HE, UK*

Received 21 December 2003; received in revised form 8 April 2004; accepted 19 April 2004

Available online 11 August 2004

Abstract

The low-temperature structures of the colquiriite-type fluorides $LiCaAlF_6$ and $LiSrAlF_6$ have been investigated by single crystal X-ray diffraction. Molecular orbital calculations were also carried out using cluster models based on the obtained structures. The crystallographic *c*-axis at 120 K in $LiSrAlF_6$ became slightly elongated with respect to the 300 K lattice and the structure became more distorted. In contrast, there was uniform lattice parameter contraction in $LiCaAlF_6$ and the structure changed minimally between 300 and 120 K. These structural variations support other studies of temperature dependent optical properties reported in the literature.

Keywords: Structure; $LiCaAlF_6$; $LiSrAlF_6$; Synchrotron; Colquiriite; Fluoride; Laser

1. Introduction

Fluorides with colquiriite-type structure, $LiCaAlF_6$ (LiCAF) and $LiSrAlF_6$ (LiSAF), are finding use as host materials for tunable solid-state lasers. Near-infrared emissions observed from Cr^{3+}-doped LiCAF and LiSAF are ascribed to a $3d$–$3d$ transition of Cr^{3+}, substitutionally replacing Al in the octahedral $2d$ sites [1,2]. Electric dipole transitions of this type are forbidden for perfect O_h octahedral symmetries, but in many materials, static and dynamic structural distortions break the degeneracies of the contributing orbitals.

In the colquiriite-type fluorides discussed here two static modes of octahedral deformation are permitted. They correspond to an even parity (symmetric) octahedral flattening or expansion mode along a single structurally enforced three-fold axis and, an odd parity, counter-rotatory mode of the octahedral faces normal to that axis [3]. The latter mode breaks the inversion symmetry of the cation site and strongly enhances the laser emission cross-section [4]. The degree of octahedral deformation within those modes varies with temperature as well as with substitutional replacement of the atomic constituents. The transition energies and lifetimes of the electronic states of the Cr^{3+} dopant can therefore be tuned to a certain extent.

LiSAF host crystals exhibit broader absorption and emission (780–1010 nm) bands than LiCAF (720–840 nm). This broadness is evidence of a vibronic transition wherein the excited states induce further localized, dynamic Jahn-Teller deformations of the octahedral environment and associated crystal field [3–7]. The broader emission range for LiSAF indicates greater configurational displacements while in the excited state.

*Corresponding author. Materials and Structures Laboratory, Tokyo Institute of Technology, Nagatsuta 4259, Midori-ku, Yokohama, 226-8503 Japan. Fax: +81-45-924-5360.
E-mail address: ishizawa@nitech.ac.jp (N. Ishizawa).

0022-4596/$ - see front matter © 2004 Elsevier Inc. All rights reserved.
doi:10.1016/j.jssc.2004.04.039

The relative stability of the excited states is expressed in terms of the emission lifetime and is influenced by both dynamic and static spontaneous transition rates as well as the rate of non-radiative decay. For LiCAF the lifetime decreases with increasing temperature, from 190 μs at 77 K to 156 μs at room temperature, whereas for LiSAF it is almost constant, being 67 μs at 77 K but increasing slightly to 70 μs at 273 K [4]. Schaffers et al. [8] suggested that the larger static distortions present in LiSAF enhance the relaxation of the Laporte symmetry transition rules, thereby leading to shorter emission lifetimes. Reasons behind the unusual temperature dependence of the LiSAF decay lifetime are not yet well understood [5]. Thermal quenching of the fluorescence lifetime by non-radiative processes occurs at around 342 K for LiSAF and up to 528 K for LiCAF so that LiCAF hosts have better thermo-mechanical stability [5].

The room temperature structures of LiCAF and LiSAF are isomorphous and described by the trigonal space group $P\bar{3}1c$ [8–11]. There is an approximately 0.15 Å increase in atomic radius from Ca to Sr and this leads to small but significant increases in structural distortion for LiSAF. Fig. 1 shows the crystal structure of LiCAF at 300 K. All metal ions are octahedrally coordinated by six fluorine atoms. The Ca and Sr octahedra are trigonally elongated along the *c*-axis. These sites have D_{3d} symmetry. The Al atoms occupy distorted octahedral sites of D_3 symmetry. The AlF_6 octahedra are slightly compressed and twisted about their rotation axes. The Li atom occupies a substantially more compressed octahedral site.

The AlF_6 and LiF_6 octahedra share edges, forming discrete layers of six membered hexagonal rings, each with a cavity at its center. The Ca or Sr atoms form intermediate layers of isolated CaF_6 or SrF_6 octahedra, stacked above and below the hexagonal cavities. Each is attached to the Li–Al layers via three corner sharing F atom apices as shown in Fig. 2.

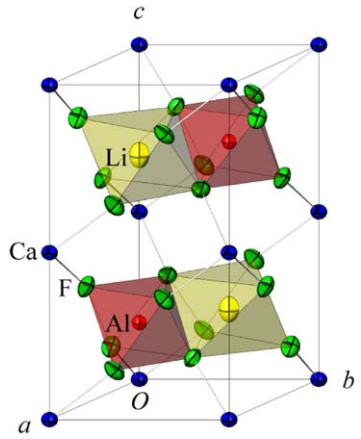

Fig. 1. The structure of LiCAF at 300 K with Ca (blue), Al (red), Li (yellow) and F (green) atoms.

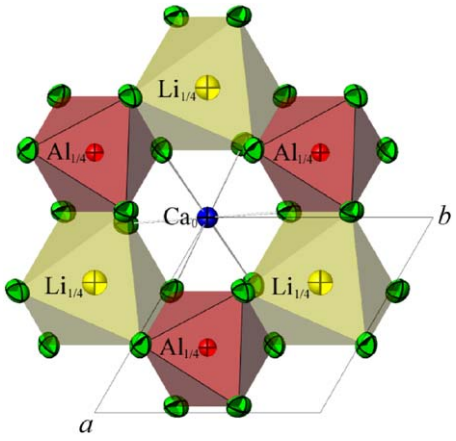

Fig. 2. The *c*-axis projection of LiCAF at 300 K. AlF_6 (red) and LiF_6 (yellow) octahedra share edges. CaF_6 octahedron (blue) share corners with AlF_6 and LiF_6 octahedra.

Given the strong sensitivity of the electronic transitions to rather minor variations of atomic structure we sought to apply high precision, single crystal, synchrotron X-ray diffraction to determine structural information of higher quality than previous work. Studies were undertaken of both LiSAF and LiCAF at 300 K and 120 K to help quantify the temperature dependence of the lattice and atomic positional and vibrational parameters. LiSAF is thought to be the first fluoride structure ever detected with a negative thermal expansion coefficient [6].

2. Experimental

Single crystals of LiCAF and LiSAF were grown containing nominally 2 at% Cr in an inert atmosphere (Ar gas) by the Czochralski technique. The pulling rate was 1 mm/h. The starting materials were prepared from commercially available fluoride powders of high purity (>99.99%). Cr^{3+} ions substitute for Al^{3+} ions, contributing a pale green color due to the otherwise transparent crystals. An EDAX EAGLE microprobe analysis, revealed no detectable impurities. Single crystals of LiCAF and LiSAF with dimensions of $17.4 \times 15.4 \times 7.7$ and $17.4 \times 17.4 \times 9.7\,\mu m^3$, respectively, were selected and mounted on the tips of tapered glass fibers.

The X-ray diffraction experiments were undertaken using a horizontal-type four-circle diffractometer mounted on beam line 14A of the Photon Factory, High Energy Accelerator Research Organization [12]. The sample temperature was controlled by an Oxford Cryosystem, dry nitrogen gas-blowing cooler and the temperature controlled within ±0.1 K. Experiments for

both LiCAF and LiSAF were undertaken at 300 and 120 K. Cell parameters were determined from 24 well-refined Bragg reflections within the range $81 \leqslant 2\theta \leqslant 92°$ for LiCAF and $78 \leqslant 2\theta \leqslant 90°$ for LiSAF using X-rays of 0.75031 Å wavelength. That value was calibrated from the known cell dimensions of a spherically ground standard Si crystal.

Intensity data were collected in the 2θ range $2\theta \leqslant 130°$ for single hemispheres in each experiment, using vertically polarized X-rays of 0.8048 Å wavelength. This wavelength was chosen to avoid the K absorption edge of Strontium (0.76973 Å). Diffracted X-rays were measured with an eight-channel avalanche photodiode detector with around 75% detection efficiency [13]. Custom designed Diff14A software was used to drive the goniometer crate. Experimental details of each experiment are summarized in Table 1. Unit cell and structural parameters were refined using the *Xtal 3.7* program packages [14]. Refined atomic coordinates and anisotropic displacement parameters are shown in Tables 2 and 3, respectively. Refinements assuming 2 at% Cr substituted at the Al site were undertaken but revealed no significant changes in the final parameters from those listed in Tables 2 and 3.

Complementary theoretical calculations were carried out using the first principles molecular orbital program SCAT [15], a modified version of the discrete variational (DV)-Xα. The cluster models $Li_6^+Ca_3^{2+}Al_6^{3+}F_{30}^-$ for LiCAF and $Li_6^+Sr_3^{2+}Al_6^{3+}F_{30}^-$ for LiSAF were chosen as Ca or Sr centered spheres of neutral charge. Cluster coordinates were generated from the atomic positions determined by X-ray diffraction in this study. The Madelung potential was taken into consideration by formal point charges at 19015 atomic sites around the cluster. Spin polarization was also considered. The atomic orbitals, 1*s* through 2*p* for Li, 1*s* through 4*p* for Ca, 1*s* through 5*s* for Sr, 1*s* through 3*d* for Al, 1*s* through 2*p* for F, were used as basis functions. The number of electrons included was 426 and 480 for the $Li_6^+Ca_3^{2+}Al_6^{3+}F_{30}^-$ and $Li_6^+Sr_3^{2+}Al_6^{3+}F_{30}^-$ clusters, respectively. Self-consistent field convergence was attained within about 30 cycles for all four calculations. Final charge shifts were all less than 0.0002 e. For each compound only very minor difference exists between the 300 and 120 K calculations.

3. Results and discussion

Table 1 contains the primary statistics reflecting the quality of the experiments. In view of the smaller atomic radii of Ca with respect to Sr, the lattice parameters of LiCAF are smaller. For each crystal, lowering the temperature reduces the volume of the unit cell as seen by the general reduction in the dimensions of *a* and *c*. The exception is the lattice parameter *c* of LiSAF which becomes slightly elongated at 120 K. Because the crystals were very small, correction for absorption assuming a spherical shape does not improve the reflection merging statistics. For LiCAF the structural refinement R-factors show that the low-temperature data give a significantly better fit to the harmonically vibrating, independent atom model (IAM). For LiSAF the reverse is true. Reducing the temperature and mean atomic displacement amplitudes worsens agreement with the IAM, although from Table 2, both crystals show a reduction of the order 1/2 in the mean atomic displacement amplitudes (U_{eq}) at 120 K.

Because Li, Al and either Sr or Ca occupy high symmetry positions in the $P\bar{3}1c$ space group, their mean

Table 1
Crystal data and experimental conditions

	$LiCaAlF_6$ 300 K	$LiCaAlF_6$ 120 K	$LiSrAlF_6$ 300 K	$LiSrAlF_6$ 120 K
Lattice parameters				
a (Å)	5.0081(2)	4.9952(2)	5.0848(1)	5.0692(1)
c (Å)	9.6433(13)	9.6430(13)	10.2173(8)	10.2354(8)
V (Å^3)	209.46(3)	208.38(3)	228.78(2)	227.78(2)
D (g cm^{-3})	2.09	2.10	2.61	2.61
Absorption coefficient (cm^{-1})	23.69	23.80	28.67	28.80
Sin θ/λ_{MAX}	1.126	1.126	1.126	1.126
2θ range (°)	1–130	1–130	1–130	1–130
Measured area	$-12 \leqslant h \leqslant 12$	$-12 \leqslant h \leqslant 12$	$-12 \leqslant h \leqslant 12$	$-12 \leqslant h \leqslant 12$
	$-12 \leqslant k \leqslant 12$	$-12 \leqslant k \leqslant 12$	$-12 \leqslant k \leqslant 12$	$-12 \leqslant k \leqslant 12$
	$0 \leqslant l \leqslant 22$	$0 \leqslant l \leqslant 22$	$0 \leqslant l \leqslant 24$	$0 \leqslant l \leqslant 24$
R_{int}	0.0481	0.0555	0.1039	0.0818
Reflections				
Measured	5117	5315	5917	5870
Independent [$F > 3\sigma(F)$]	614	627	725	740
R_F	0.0322	0.0211	0.0328	0.0354
R_{wF}	0.0353	0.0209	0.0316	0.0313

Table 2
Fractional atomic coordinates and isotropic atomic displacement parameters

Atom	Site		$LiCaAlF_6$ 300 K	$LiCaAlF_6$ 120 K	$LiSrAlF_6$ 300 K	$LiSrAlF_6$ 120 K
Li	2*c* (1/3 2/3 1/4)	U_{eq} (Å^2)	0.015(2)	0.012(2)	0.021(2)	0.011(2)
Ca/Sr	2*b* (0 0 0)	U_{eq} (Å^2)	0.0083(1)	0.00495(7)	0.01137(8)	0.00556(8)
Al	2*d* (2/3 1/3 1/4)	U_{eq} (Å^2)	0.0069(2)	0.0045(1)	0.0092(2)	0.0049(3)
F	12*i*	*x*	0.3767(2)	0.3764(1)	0.3880(2)	0.3868(2)
		y	0.0310(2)	0.0300(1)	0.0317(2)	0.0305(2)
		z	0.14336(7)	0.14338(4)	0.14850(6)	0.14874(6)
		U_{eq} (Å^2)	0.0121(3)	0.0071(2)	0.0176(4)	0.0090(3)

Table 3
Anisotropic atomic displacement parameters

	U_{11} (Å^2)	U_{22} (Å^2)	U_{33} (Å^2)	U_{12} (Å^2)	U_{13} (Å^2)	U_{23} (Å^2)
Li						
$LiCaAlF_6$ 300 K	$2U_{12}$	$2U_{12}$	0.022(2)	0.0062(8)	0	0
$LiCaAlF_6$ 120 K	$2U_{12}$	$2U_{12}$	0.013(1)	0.0054(5)	0	0
$LiSrAlF_6$ 300 K	$2U_{12}$	$2U_{12}$	0.025(2)	0.0098(9)	0	0
$LiSrAlF_6$ 120 K	$2U_{12}$	$2U_{12}$	0.014(2)	0.0049(8)	0	0
Ca/Sr						
$LiCaAlF_6$ 300 K	$2U_{12}$	$2U_{12}$	0.0071(1)	0.00445(4)	0	0
$LiCaAlF_6$ 120 K	$2U_{12}$	$2U_{12}$	0.00492(7)	0.00248(2)	0	0
$LiSrAlF_6$ 300 K	$2U_{12}$	$2U_{12}$	0.00897(7)	0.00628(3)	0	0
$LiSrAlF_6$ 120 K	$2U_{12}$	$2U_{12}$	0.00534(7)	0.00283(3)	0	0
Al						
$LiCaAlF_6$ 300 K	$2U_{12}$	$2U_{12}$	0.0076(2)	0.00330(8)	0	0
$LiCaAlF_6$ 120 K	$2U_{12}$	$2U_{12}$	0.0056(2)	0.00195(5)	0	0
$LiSrAlF_6$ 300 K	$2U_{12}$	$2U_{12}$	0.0107(2)	0.00424(8)	0	0
$LiSrAlF_6$ 120 K	$2U_{12}$	$2U_{12}$	0.0065(2)	0.00206(8)	0	0
F						
$LiCaAlF_6$ 300 K	0.0116(2)	0.0098(2)	0.0130(2)	0.0040(2)	−0.0049(2)	−0.0017(2)
$LiCaAlF_6$ 120 K	0.0066(1)	0.0059(1)	0.0082(1)	0.0026(1)	−0.0022 (1)	−0.0006(1)
$LiSrAlF_6$ 300 K	0.0167(3)	0.0130(3)	0.0194(2)	0.0048(2)	−0.0084(2)	−0.0016(2)
$LiSrAlF_6$ 120 K	0.0084(2)	0.0067(3)	0.0103(2)	0.0026(2)	−0.0037(2)	−0.0005(2)

positions and mean harmonic displacements are very restricted. They all possess cylindrical symmetry about the hexagonal three-fold axes. The F anion occupies a site of general symmetry with no positional restrictions and therefore has the largest positional freedom. Of the 15 free structural parameters in the IAM, 9 describe fluorine. Table 2 shows that the temperature dependence of the F atom coordinates vary by at most a factor of 0.001*a* for each of LiCAF and LiSAF. On the other hand, variations between these structures are 10 times larger, differing by up to 0.01*a*.

The anisotropic temperature factors determined from each experiment are shown in Table 3. With the exception of the Li atoms, and in agreement with the U_{eq} values, there is an almost uniform reduction by 1/2 in the U_{ij} values of the 120 K experiments. The only discrepancy is for U_{12} of Li, but given its low atomic number and mass, a degree of insensitivity is tolerable for this atom. The atomic coordinates and displacement parameters refined for each crystal do not suggest any unusual structural behavior.

Interatomic distances and angles are presented in Table 4. They agree reasonably with previous structural reports [8–11]. The Al–F distances in both compounds remain almost constant with temperature. These bonds are the shortest and strongest in the structure. This adds an extra degree of rigidity to the AlF_6 octahedra with respect to other structural modifications. The Sr–F bondlengths in LiSAF are about 0.15 Å longer than the Ca–F bonds in LiCAF, in accordance with the differences in ionic radii. At 120 K both bonds shrink appreciably, by 0.0032(7) Å for Ca–F and 0.0037(8) Å for Sr–F. There is a 0.0079(7) Å contraction of the Li–F bonds at 120 K for LiCAF and a 0.0084(8) Å contraction in LiSAF.

The interatomic bond angles in Table 4 also strongly reflects the relative labilities of the respective Li, Al and Sr/CaF_6 octahedra. In each experiment the F–Al–F angles show the smallest variation, approximately 5° and 9° for LiCAF and LiSAF, respectively. The F–Ca/Sr–F angles vary by about 1° more, while angular variations of the LiF_6 octahedra are of the order 13° in

Table 4
Selected interatomic bondlengths (Å) and angles (°)

	$LiCaAlF_6$ 300 K	$LiCaAlF_6$ 120 K	$LiSrAlF_6$ 300 K	$LiSrAlF_6$ 120 K
Li–F	2.0095(7) × 6	2.0016(4) × 6	2.0205(7) × 6	2.0121(8) × 6
Ca/Sr–F	2.2807(7) × 6	2.2775(4) × 6	2.4294(8) × 6	2.4257(8) × 6
Al–F	1.8055(7) × 6	1.8053(4) × 6	1.8062(8) × 6	1.8071(8) × 6
Al–Ca/Sr	3.7646(2) × 6	3.7588(2) × 6	3.8914(1) × 6	3.8876(1) × 6
F–F/LiF_6 ⊥	2.9903(7) × 6	2.9746(4) × 6	3.0034(8) × 6	2.9873(8) × 6
F–F/LiF_6	2.4825(7) × 3	2.4791(4) × 3	2.4480(8) × 3	2.4478(8) × 3
F–F/LiF_6	2.8984(7) × 3	2.8892(4) × 3	2.9760(8) × 3	2.9614(8) × 3
F–F/(Ca/Sr)F_6 ⊥	3.1419(7) × 6	3.1347(4) × 6	3.2864(8) × 6	3.2706(8) × 6
F–F/(Ca/Sr)F_6	3.3069(7) × 6	3.3048(4) × 6	3.5789(8) × 6	3.5830(8) × 6
F–F/AlF_6 ⊥	2.5703(7) × 6	2.5701(4) × 6	2.5613(8) × 6	2.5642(8) × 6
F–F/AlF_6	2.4825(7) × 3	2.4791(4) × 3	2.4480(8) × 3	2.4478(8) × 3
F–F/AlF_6	2.5910(7) × 3	2.5936(4) × 3	2.6506(8) × 3	2.6504(8) × 3
F–Li–F	96.15(3) × 6	95.98(2) × 6	96.02(3) × 6	95.86(3) × 6
	92.30(3) × 3	92.39(2) × 3	94.86(3) × 3	94.77(3) × 3
	76.29(3) × 3	76.53(2) × 3	74.58(4) × 3	74.93(3) × 3
F–(Ca/Sr)–F	92.93(3) × 6	93.03(2) × 6	94.88(3) × 6	95.22(3) × 6
	87.07(3) × 6	86.97(2) × 6	85.12(3) × 6	84.78(3) × 6
F–Al–F	90.76(4) × 6	90.77(2) × 6	90.31(4) × 6	90.38(4) × 6
	91.71(4) × 3	91.84(2) × 3	94.40(4) × 3	94.33(4) × 3
	86.86(4) × 3	86.73(2) × 3	85.33(4) × 3	85.26(4) × 3

The mark ⊥ indicates bonds normal to *c*.

LiCAF and 15° in LiSAF. This again points to a robust AlF_6 geometry.

Structural distortions within compounds containing octahedra can be characterized in a variety of ways. Collective behaviors of the octahedral vertices leading to static rotations (tilting) of the octahedra about an axis provide one measure of distortion. Only one rotation axis is possible for the three independent MF_6 octahedra because each possesses a symmetry enforced three-fold axis. From Fig. 2 it is clear that neither the AlF_6 or LiF_6 octahedra are rotated about their three-fold axes. On the other hand, the CaF_6 and SrF_6 octahedra are tilted by about 4.5°, an amount reflecting the disproportionate sizes of the AlF_6 and LiF_6 octahedra.

When a single three-fold symmetry axis is preserved for an octahedron it may be more usefully described in terms of a triangular antiprism, with two perfect equilateral triangular (anti)-faces oriented normal to the three-fold axis. Then the distance between those faces can be defined as the octahedral height *h*, as shown in Fig. 3. Table 5 contains values of *h* for all three octahedra in each experiment. The heights of the LiF_6 and AlF_6 octahedra are identical owing to their colayering and mutual edge sharing. Their heights are also almost constant with temperature for each compound. So too is the height of the CaF_6 octahedra. The one exception is the SrF_6 octahedra whose height increases from 3.0345(8) Å at 300 K to 3.0450(8) Å at 120 K. With two SrF_6 layers in the unit cell this summed increase is identically the 0.018 Å increase in the LiSAF unit cell lattice parameter *c*. The absence of a corresponding change in CaF_6 height is therefore quite in accordance with the very minor 0.0003(13) Å decrease in the corresponding LiCAF cell parameter at 120 K.

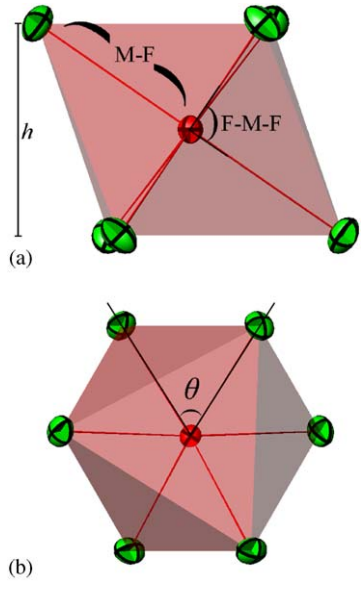

Fig. 3. Definition of *h* (a) and *θ* (b). The "*h*" is a height of octahedron along the *c*-axis direction, M–F is a bond length, F–M–F is a bond angle. The antiphase angle is denoted by "*θ*".

The variation of octahedral height along the three-fold axis can be contrasted with variations of an

Table 5
Characteristic parameters with definitions given in the text

	$LiCaAlF_6$ 300 K	$LiCaAlF_6$ 120 K	$LiSrAlF_6$ 300 K	$LiSrAlF_6$ 120 K
BVS: Li	1.05	1.07	1.02	1.04
Net charge: Li	0.82	0.82	0.82	0.82
h: LiF_6 (Å)	2.0563 (14)	2.0563 (8)	2.0741 (12)	2.0727 (12)
θ: LiF_6 (°)	72.51	72.45	75.96	75.64
DI: F–Li–F	7.864×10^{-2}	7.728×10^{-2}	8.978×10^{-2}	8.767×10^{-2}
$1+\zeta$	0.8424 (7)	0.8466 (4)	0.8464 (6)	0.8496 (6)
BVS: Ca/Sr	1.85	1.87	2.01	2.03
Net charge: Ca/Sr	1.76	1.76	1.90	1.90
h: (Ca/Sr)F_6 (Å)	2.7653 (14)	2.7652 (9)	3.0345 (12)	3.0450 (13)
θ: (Ca/Sr)F_6 (°)	60	60	60	60
DI: F–(Ca/Sr)–F	3.256×10^{-2}	3.367×10^{-2}	5.422×10^{-2}	5.800×10^{-2}
$1+\zeta$	1.0779 (7)	1.0805 (4)	1.1316 (6)	1.1405 (6)
BVS: Al	2.99	3.00	2.99	3.00
Net charge: Al	1.89	1.89	1.89	1.88
h: AlF_6 (Å)	2.0563 (14)	2.0563 (8)	2.0741 (12)	2.0727 (12)
θ: AlF_6 (°)	64.14	64.36	67.84	67.81
DI: F–Al–F	1.769×10^{-2}	1.847×10^{-2}	2.692×10^{-2}	2.731×10^{-2}
$1+\zeta$	0.9803 (8)	0.9800 (4)	0.9923 (7)	0.9899 (7)
BVS: F	0.98	0.99	1.00	1.01
Net charge: F	−0.70	−0.70	−0.73	−0.73

equivalent ideal octahedron of similar edge length using the notion of octahedral strain formulated by Megaw and Darlington [16]. This conveniently parameterizes the even parity deformation mode of the AlF_6 octahedra. Taking the mean F–F distance l of the six edges of the octahedral antifaces as a reference (denoted $\perp$ in Table 4), the height of an ideal octahedra of equal side length is just $h_i = l \times \sqrt{2/3}$. Variations from that ideal are characterized by the octahedral strain ξ formulated as

$$1 + \xi = h/h_i = (h/l) \times \sqrt{3/2}.$$

When $\zeta < 0$ the octahedra is flattened along the three-fold axis and conversely $\zeta > 0$ implies elongation. Values of the octahedral strain shown in Table 5 shows that the LiF_6 octahedra is severely strained with almost constant 15% flattening in each experiment. In contrast the CaF_6 and SrF_6 octahedra are elongated by 8% and 13%, respectively. For LiSAF the strain increases to 14% when the temperature is reduced to 120 K whereas the equivalent increase is only by 0.2% for LiCAF.

Electron spin resonance (ESR) measurements by Yamaga et al. [7] indicate that the Cr doped AlF_6 environment in LiCAF should be compressed along the c-axis and this agrees qualitatively with the 2% negative octahedral strain observed here. They also predicted that with decreasing temperature the magnitude of the octahedral strain should increase slightly for LiCAF, though within one sigma in our observation. With regard to LiSAF, the ESR results suggest that the $Cr^{3+}F_6$ octahedra is elongated with positive strain which increases at higher temperature. Certainly the 1% negative strain measured here for LiSAF is more positive than the LiCAF equivalent and the strain is closer to positive at 300 K than at 120 K by three sigma. The structural trends reported by Yamaga et al. therefore seem to be born out, even though precise values differ. It should not be overlooked that the ESR experiments selectively probe the Cr^{3+} sites which are likely to differ slightly from the AlF_6 environment of the bulk.

The odd parity octahedral deformation mode can be characterized in terms of variations from the ideal 60° phase relationships between vertices of the triangular antifaces (illustrated in Fig. 3b) normal to the three-fold axis. These differences reflect differential torques applied at each end of the triangular antiprism. For the CaF_6 and SrF_6 octahedra the phase angle (θ) is identically 60° indicating pure rotation rather than deformation. The LiF_6 octahedra show the greatest deformation, with phase shifts of up to 71°, whereas the AlF_6 octahedra are deformed more modestly. In LiCAF the deformation does not change with temperature, but in LiSAF it relaxes very slightly from 67.84° to 67.81° at 120 K.

A more general method of quantifying octahedral deformation follows from the bondangle distortion indices, (DI) of Baur et al. [17];

$$\mathrm{DI} = \left(\sum |\varphi - \varphi_i|\right)/n\varphi_i,$$

where φ is each bondangle, φ_i is the ideal bondangle of the regular polyhedron (109.4° for tetrahedra, 90° for octahedra) and n is the number of bonds. The AlF_6 DI values for both compounds are larger at low-temperature. The LiF_6 octahedra in LiCAF and LiSAF are both more distorted at 300 K but the $(Ca/Sr)F_6$ octahedra are less distorted at that temperature.

The angular distortion indices show that the AlF_6 octahedra in LiCAF are more perfect at 300 K than 120 K, whereas the Cr^{3+} emission lifetime in LiCAF is shorter at room temperature than at low-temperature. Presumably the locally increased thermal vibrations at room temperature enhance the dynamical transition rate sufficiently to offset the more nearly perfect average octahedral symmetry and weakened relaxation of the Laporte selection rules. In LiSAF the largely temperature independent emission rate may arise from the complementary way that the even-parity strain mode of the AlF_6 and CrF_6 octahedra tends toward more positive values as the vibrational motion and temperature decrease.

Bond valence sums [18] can provide strong signals of structural anomalies or errors in ionic lattices. The BVS is defined as

$$\sum \exp[(r_0 - r_{ij})/0.37],$$

where r_0 is an empirically determined parameter for each cation–fluorine bond [19] and r_{ij} is the bondlength between the cation and jth coordinating fluorine atom. Sums determined for all anions and cations in LiSAF and LiCAF agree well with commonly assumed atomic valences. The BVS for Ca differs significantly more from the formal value than it does for Sr. The low BVS for Ca indicates underbonding and could indicate a degree of bond-strain elsewhere in the structure. Atomic charges were also determined from the molecular orbital (MO) calculations and these show trends similar to the BVS. There are many different methods of assigning and partitioning atomic charges, so precise MO charges inevitably differ from the corresponding formal ionic values, even though the relative values are quite consistent with expectations.

From the MO calculations, the 3p energy levels of Ca^{2+} in LiCAF (−18.1 eV) are lower than the 4p energy levels of Sr^{2+} in LiSAF (−13.7 eV). Therefore, those orbitals of Ca mix more strongly with the valence orbital of F than Sr, as shown in Fig. 6. Since the Sr–F bond in LiSAF is more ionic than Ca–F bond in LiCAF, the fluorine atoms in LiSAF have larger charge than in LiCAF as shown in Table 5. The BVS value of fluorine in LiSAF is also larger than in LiCAF.

We have previously considered the lattice as a set of discrete connected octahedra. In reality though it is the F anions that link these octahedra together. Each F atom adopts an almost trigonal planar coordination to each of Al, Li and Ca or Sr for LiCAF and LiSAF,

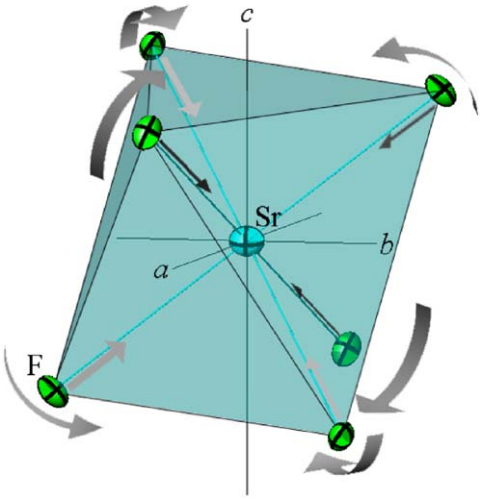

Fig. 4. Distortion of SrF_6 octahedron (blue) from 300 to 120 K.

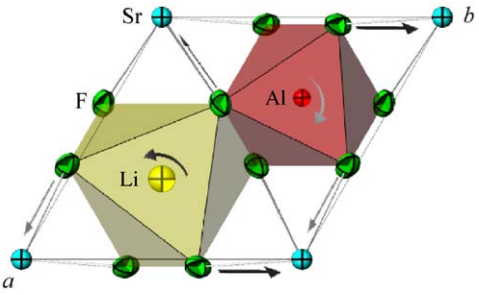

Fig. 5. Distortions of AlF_6 octahedron (red) and LiF_6 octahedron (yellow) at 120 K.

respectively. With decreasing temperature the strength of the Sr–F bonds increases and they become shorter at the expense of the competing Li–F bonds that become longer and weaker. The curious feature is that despite the decrease in Sr–F bondlengths, the SrF_6 octahedra become more elongated leading to the net increase in length of the c-axis, as shown in Fig. 4. Structurally there is no clear explanation for this. It does not arise from direct steric hindrance because the F–F contacts defining the perimeter of the SrF_6 unit are significantly larger than those around the AlF_6 octahedra. The tensions created between the F–Al and F–Li bonds by the foreshortening of the F–Sr bonds are constrained purely within the Al/LiF_6 layers and therefore should have no direct effect on the SrF_6 elongation. This is particularly salient given the absence of such deformation modes in CaF_6, despite similar but slightly smaller Ca–F bondlength foreshortening. The implications are that the observed elongation could arise from bonding orbital repulsions due to geometric overcrowding at the Sr atom sites, or due to strengthened F–F repulsions between adjacent Al/LiF_6 layers (Fig. 5).

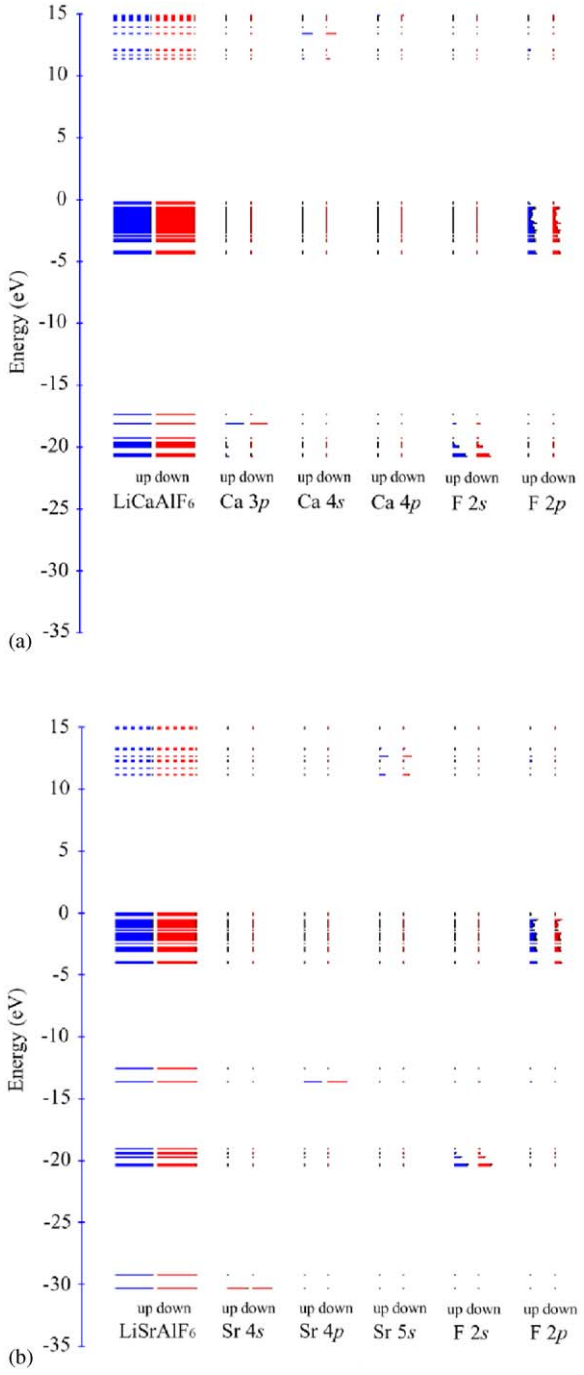

Fig. 6. The energy level structures of the molecular orbitals (leftmost) and the atomic orbitals (right) for Ca, Sr and F atoms for LiCAF (a) and LiSAF (b).

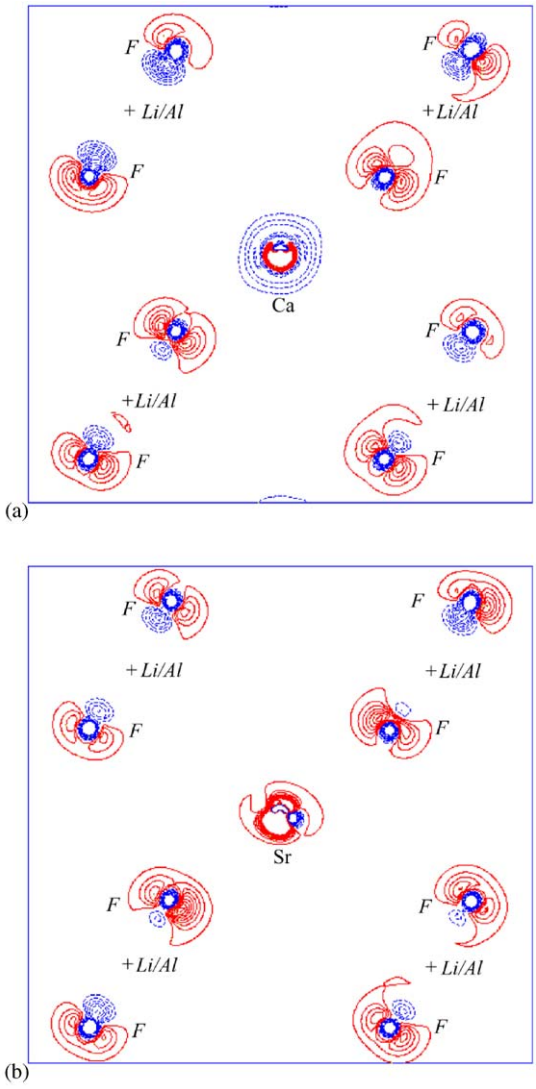

Fig. 7. The calculated difference electron density distribution on (010) for LiCAF (a) and LiSAF (b) with contour intervals of 0.025 e Å^{-3}. The Ca/Sr atoms lie on the plane while F atoms are displaced perpendicularly from the plane by 0.13–0.14 Å, and Li/Al atoms by 1.44–1.46 Å. Red and blue lines indicate excess and depleted electron density.

The difference electron density distributions obtained from MO calculations for LiCAF and LiSAF are shown in Fig. 7. Greater accumulations of electron density exist around the fluorine atoms in LiSAF than in LiCAF. This is also reflected by the F atom charges shown in Table 5. The orientations of those accumulations are broadly directed around the perimeter of the AlF_6 and LiF_6 octahedra. This suggests enhancement of the repulsive forces between adjacent AlF_6–LiF_6 layers and directed along the *c*-axis. The spacing between those layers is identically *h* for SrF_6 as listed in Table 5 and the F–F contacts involved are the edges of the SrF_6 octahedron contained in Table 4. This could be the source of the structural differences between LiCAF and LiSAF and the negative thermal expansion coefficient along the *c*-axis.

4. Summary

With the exception of *c* for LiSAF, all cell dimensions shrank with temperature from 300 to 120 K. The different temperature dependency of the cell parameters

is reflected most strongly in the differing degrees of CaF_6 and SrF_6 octahedral strain. The shape of the AlF_6 octahedra in LiCAF barely changes between 300 and 120 K, whereas in LiSAF, the octahedral strain changes by a factor around 10 times larger between those temperatures. The fluorine atom charges in LiSAF are larger than in LiCAF and this could give rise to stronger repulsions between AlF_6–LiF_6 adjacent layers. In LiCAF, the room temperature emission lifetime is shorter than at low temperature because the increased thermal vibration of atoms with temperature assists the vibronic transition rate. In LiSAF, the temperature-independent emission arises from the decrease in AlF_6 structural distortion as the temperature increases which reduces the accessibility of the vibronic transition modes.

Acknowledgments

This study was supported by Grant-in-Aid for Scientific Research No. 14550663 from The Ministry of Education, Science, Sports and Culture of Japan, and by the Inter-University Cooperative Research Program of the Materials and Structures Laboratory, Tokyo Institute of Technology. DDB acknowledges JSPS fellowship P02148. The measurement was carried at the Photon Factory, KEK, based on the program 2002G042.

References

[1] S.A. Payne, L.L. Chase, H.W. Newkirk, L.K. Smith, IEEE J. Quantum Electron. 24 (1988) 2243–2252.
[2] S.A. Payne, L.L. Chase, L.K. Smith, W.L. Kway, H.W. Newkirk, J. Appl. Phys. 66 (1989) 1051–1056.
[3] H.W.H. Lee, S.A. Payne, L.L. Chase, Phys. Rev. B 39 (1989) 8906–8914.
[4] S.A. Payne, L.L. Chase, G.D. Wilke, J. Lumin. 44 (1989) 167–176.
[5] M. Stalder, M. Bass, B.H.T. Chai, J. Opt. Soc. Am. B 9 (1992) 2271–2273.
[6] M. Stalder, B.H.T. Chai, M. Bass, Appl. Phys. Lett. 58 (1991) 216–218.
[7] M. Yamaga, B. Henderson, K. Holliday, T. Yoshida, M. Fukui, K. Kindo, J. Phys.: Condens. Matter 11 (1999) 10449–10510.
[8] K.I. Schaffers, D.A. Keszler, Acta Crystallogr. C 47 (1991) 18–20.
[9] Y. Ono, K. Nakano, K. Shimamura, T. Fukuda, T. Kajitani, J. Cryst. Growth 229 (2001) 505–509.
[10] N.B. Bolotina, B.A. Maksimov, V.I. Simonov, S.I. Derzhavin, T.V. Uvarova, V.V. Apollonov, Kristallografia 38 (1993) 43–50.
[11] V.W. Viebahn, Z. Anorg. Allg. Chem. 386 (1971) 335–339.
[12] Y. Satow, Y. Iitaka, Rev. Sci. Instrum. 60 (1989) 2390–2393.
[13] S. Kishimoto, N. Ishizawa, T.P. Vaalsta, Rev. Sci. Instrum. 69 (1998) 384–391.
[14] S.R. Hall, D.J. du Boulay, R. Olthof-Hazekamp (Eds.), Xtal 3.7. University of Western Australia. Web address: http://Xtal.crystal.uwa.edu.au/, 2000.
[15] H. Adachi, M. Tsukada, C. Satoko, J. Phys. Soc. Japan 45 (1978) 875–883.
[16] H.D. Megaw, C.N. Darlington, Acta Crystallogr. A 31 (1975) 161–173.
[17] W.H. Baur, Acta Crystallogr. B 30 (1974) 1195–1215.
[18] I.D. Brown, D. Altermatt, Acta Crystallogr. B 41 (1985) 244–247.
[19] N.E. Brese, M. O'Keeffe, Acta. Crystallogr. B 47 (1991) 192–197.